Defence Technology 17 (2021) 429–439

Contents lists available at ScienceDirect

Defence Technology

journal homepage: www.keaipublishing.com/en/journals/defence-technology

Research progress on advanced rail materials for electromagnetic railgun technology

Hong-bin Xie [a, b], Hui-ya Yang [a, b], Jian Yu [a], Ming-yu Gao [a, b], Jian-dong Shou [a, b], You-tong Fang [b], Jia-bin Liu [a, b, *], Hong-tao Wang [b, **]

[a] School of Materials Science and Engineering, Zhejiang University, Hangzhou, 310027, China
[b] Center for X-mechanics, Faculty of Engineering, Zhejiang University, Hangzhou, 310027, China

ARTICLE INFO

Article history:
Received 26 January 2020
Received in revised form
9 March 2020
Accepted 24 March 2020
Available online 31 March 2020

Keywords:
Strength
Conductivity
Electromagnetic railgun
Copper alloys
Rail

ABSTRACT

Electromagnetic railgun attracts more and more attention due to its advantage in speed, cost, and obscurity. It is found that the rail should withstand huge mechanical and thermal shocks during the launching operation. The forms of rail failure are accompanied by gouge, grooving, transition, and arc ablation, etc. The service life of the rail has become a bottleneck restricting the development of electromagnetic railgun technology. A series of researches are carried out to solve rail failure, including analysing the failure mechanism and using various advanced rail materials. This paper provides a comprehensive review of rail materials, including material composition, preparation, microstructure, and properties. We begin from a short background of the requirement of the rail material. Then a detailed investigation of rail materials is described, and the performances of those materials are introduced. Finally, further development prospect of rail material is discussed.

1. Introduction

The railgun is a typical electromagnetic launcher, using the thrust from magnetic force instead of the gaseous-medium gas pressure of traditional cannon to accelerate a projectile to super high speed about 2–3 km/s [1], breaking through the speed limit of traditional cannon. The railgun platform has advantages of large firepower input, large bomb storage and flexible combat use. Therefore, its military application potential is very large, and it has become an increasingly important part in the future weapon systems. The railgun mainly consists of one power source, two parallel long straight conductive rails, and a small mass armature which places between the rails as a projectile. When the two rails are connected to the power supply, a strong current is injected from one rail and flow back from the other rail through the armature to generate a strong magnetic field, as shown in Fig. 1. Meanwhile, the armature is accelerated by Ampere's force generated by electromagnetic fields. There are three major problems in the development of electromagnetic railguns, namely erosion protection of rail, miniaturization of the energy storage system, and integrated guided projectile for continuous firing [1]. Erosion protection of rail, as the first problem facing the engineering of electromagnetic railguns, is a bottleneck that must be solved in its application. The performance of the conductive rail material determines the lifetime of erosion protection. Many researches were focused on the design of advanced rail materials.

During the launching operation, the rails experience high electrical current density, large electromagnetic loads and huge mechanical and thermal shock. Under these extreme physical conditions, the forms of rail failure are accompanied by gouge, grooving, transition, and arc ablation, etc. These failures greatly reduce the service life of the rail and have become a bottleneck restricting the development of electromagnetic railgun technology.

2. Different forms of rail failure

Failure refers to the phenomenon that equipment and its components lose their original prescribed functions due to factors such as stress, time, temperature, and environmental media during use. A series of researches have been carried out to analyze failure

* Corresponding author. School of Materials Science and Engineering, Zhejiang University, Hangzhou, 310027, China.
** Corresponding author.
E-mail address: htw@zju.edu.cn (H.-t. Wang).
Peer review under responsibility of China Ordnance Society

https://doi.org/10.1016/j.dt.2020.03.014

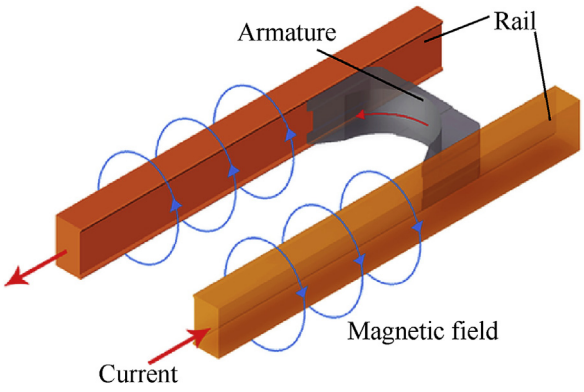

Fig. 1. Schematic of an electromagnetic railgun.

mechanism, find the cause of failure and preventive measures, and improve the material performance to extend the life of the railgun.

2.1. Gouge

Gouge mainly refers to the relative shear movement of the armature between the rails at high speed. When the yield strength of the rail material cannot withstand a huge impact and a portion of the rail would be sheared off. As shown in Fig. 2 [2], a teardrop-shaped gouge was produced on the surface. A large-volume material exfoliated due to the instantaneous high temperature and the frictional impact of the armature in a local high-strain physical environment on the local surface of the rail.

Graff and Dettloff [3] first reported gouges during high-speed rocket sleds tests in the 1960s. At that time, they considered gouge as a damaging phenomenon occurring under the conditions of high-velocity sliding contact. The first paper devoted to gouge in railgun was published in 1982 by Barber and Bauer [4]. They concluded that most gouges were caused by the interaction of microscopic asperities. Gouge was a threshold phenomenon, in that, for any given material pair, there was a threshold velocity below which gouge did not occur [5]. An investigation by Tarcza and Weldon in 1997 [6] indicated that the threshold velocity was proportional to the yield strength and hardness of the material involved. Their research showed that gouge was possible to occur even at low relative sliding velocities. Stefani and Parker [5] in 1999 reported the onset of gouge was governed by the hardness of the harder material and by the densities and sound speeds of both materials. Their experimental results showed the existence of a straight line fit between the hardness of the harder material and the shock pressure for a normal collision at the gouge threshold velocity. Schneider [7] in 2006 used several techniques (separating sabot, modified rails, and contact materials) to improve the gouge threshold velocity significantly. Watt [2] in 2011 observed that precoating the conductors of a railgun could delay the onset of gouge significantly.

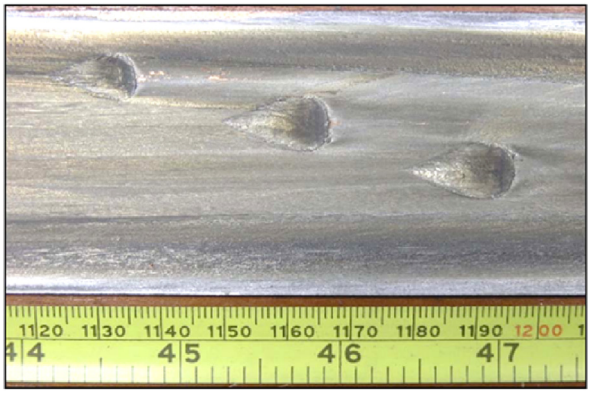

Fig. 2. Gouges on the surface of copper alloy rails. Gouges are typically teardrop-shaped [2].

2.2. Groove

Groove occurs on both sides of the rail corresponding to the position of the armature edge, and its position changes little with the number of shots, as shown in Fig. 3 [8]. Grooving pits usually start sharper and then gradually spread with cumulative effects. The groove occurs during the initial phase of the launch and extends forward along the edge of the orbit. The initial groove is caused by thermal softening and yield deformation of the material under thermal stress. Later, as the temperature rises and the armature melts, molten aluminium accelerates the corrosion of copper rails to form grooves.

Grooving damage was first observed at the University of Texas at Austin in 2001 by Gee and Persad [9]. They attributed the grooving damage to plastic deformation but did not rule out other processes. The research results of Meger et al. [10] in 2005 showed that the sliding aluminium interface provided an electrical contact which was dependent upon the location along both the length and width of the rail. They concluded that the rail itself was damaged due to localized heating enhanced by the velocity skin effect [11]. A proposed mechanism for grooving by Cooper et al. [12] in 2006 was the dissolution of the rail material into molten aluminium. Watt et al. [13] presented evidence that grooving was caused by aluminium liquid erosion instead of plasma heating or mechanical deformation.

2.3. Transition and arc ablation

A transition occurs when the armature separates from the rail, and the contact changes from perfect solid contact to arc contact, as shown in Fig. 4. The ablation power may increase nearly 100 times while the transition occurs, which leads to the rapid destruction of the conductor surface [14]. The transition also causes a series of problems such as reducing launch efficiency, destroying insulation materials, and damaging to rails. In short, the transition is very harmful to the electromagnetic launch, which should be eliminated [15]. When the transition occurs, the muzzle voltage increases, the muzzle resistance becomes larger, and the current decreases. The transition point often appears in the area where the current drops to 80%–90% of the peak value.

In 1990, Parks [16] first developed a melt-wave model for a solid armature. Melt wave started at the rear of the armature, where a current was concentrated by velocity skin effect and propagated forward along with the rail/armature interface. Many other scholars carried out further studies [17,18] on this theory with numerical calculation as the main method. Another mechanism has been put forward that changes in related mechanical properties and electrical contact characteristics lead to transition. Stefani et al. [19] in 2001 explored an “electrodynamic transition” theory. The molten aluminum layer would be pulled out of the contact surface of the pivot rail under the action of Lorentz force during the current decline stage, resulting in transition. Barber and McNab [20] in 2003 established a model that predicted the conditions under which blow-off would occur, and they found magnetic blow-off forces might lead to the transition. Satapathy and Vanicek [21] in 2006 established a 3-D model, which indicated that as applied current decreased in amplitude during the current down-slope, the

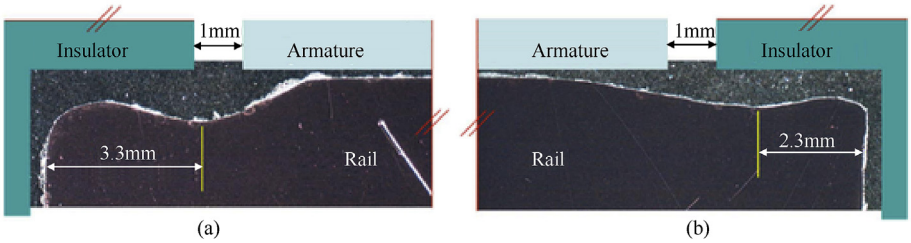

Fig. 3. Grooves at positions of armature and insulator with respect to rail edges. (a) Top edge. (b) Bottom edge [8].

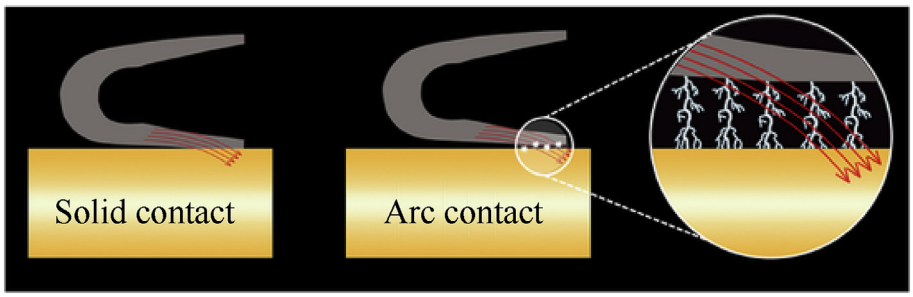

Fig. 4. A schematic diagram of the transition.

local current density and magnetic body-force density reversed in direction. Tang et al. [15] in 2017 found that the melting wave and electromagnetic force led to the occurrence of transition together. The melting wave would enlarge the separating electromagnetic force to accelerate the melting wave. The transition prediction method will be more accurate when combining the melt-wave and the electromagnetic force.

2.4. Requirements of the rail materials

The rail environment consists of large electrical currents, high local temperatures, large electromagnetic loads, and high sliding velocities [22]. When choosing rail material, two objectives for railgun must be met. One is maximizing magnetic efficiency, and the other is maximizing durability. The magnetic efficiency can be maximized by minimizing the electrical resistivity, and the rail durability is dependent on different forms of rail failure. Based on the analysis and summary of the above failure mechanism, we can obtain the performance requirements for the rail material: high electrical conductivity, high hardness, high thermal conductivity and high resistance to abrasion and arc ablation.

3. Advanced rail materials

During the research of electromagnetic guns for more than 50 years, many researchers have tried single materials and composite materials as electromagnetic launch rail. A series of research progresses are obtained to deepen the learning of the service characteristics of electromagnetic launch rail. The conducting rails of most electromagnetic launchers have historically been copper-based, such as electrolytic tough pitch copper and oxygen-free high conductivity copper [23–25] which are relatively pure metals. Pure copper is rather soft with coarse grains and many methods are adopted to refine the grain to strengthen pure copper. High-pressure torsion and nano-twinning are two effective strengthening manners [26,27]. Considering there is large thermal shocking during electromagnetic emission, the relative low softening temperature is another bottleneck for the application of pure copper. Improved performance has been sought through alloys such as Cu-Cr [28–30], Cu-Cr-Zr [31], Cu–Mo, Cu–W [32] with an alloying method, Cu/Al_2O_3 [33,34] with a composite method and application of appropriate coatings on the copper [32,35].

3.1. Copper alloys

Copper alloys are widely used in industrial fields as conductive materials because of their excellent electrical and thermal conductivity. However, with the rapid development of the electronic and electrical industries, higher requirements have been placed on the high strength and high conductivity of copper alloys. At present, most of methods improve the mechanical properties by sacrificing conductivity to a certain extent, such as the alloying method and composite material method. The alloying method is to strengthen the matrix by means of solid solution strengthening, precipitation strengthening, fine grain strengthening, and deformation strengthening. In the actual production and application of high-strength and high-conductivity alloys, the use of a single strengthening method is often very limited, so most of them are combined with each other to achieve the ultimate goal. The composite method is to strengthen the copper matrix by adding second-phase particles, whiskers, or fibers.

3.1.1. Cu–Cr

Cr has low solid solubility in Cu. About 1.28 wt% of Cr is soluble in Cu at about 1080 °C, and Cr is almost insoluble below 600 °C. So Cu–Cr alloys are actually two-phase pseudo alloys. According to the conductivity theory, the conductivity of Cu alloys is mainly related to the supersaturated solute atoms in the matrix and has little to do with dislocations and grain boundaries. Therefore, the effects of the various strengthening methods on the conductivity of Cu–Cr are obviously different. Table 1 lists the mechanical properties and electrical conductivity of the alloys under different strengthening methods.

The Cu–Cr alloy is a typical kind of aging hardening alloy. Therefore, a series of metastable phases will be precipitated in the early stage of aging. The crystal structure of the phase is consistent

Table 1
Mechanical properties and electrical conductivity of alloys with different preparation methods.

Preparation	Alloy composition /(wt.%)	Mechanical properties			Conductivity	
		Strength /MPa	Elongation /%	Hardness /(HV)	%IACS	Ref.
Casting + Cold deformation + heat treatment	Cu-0.5Cr	352	29	/	82.5	[36]
	Cu-0.8Cr	350	2.14	126	80	[37]
	Cu-0.89Cr-0.44Ag	541.5	/	205	83.2	[38]
Mechanical alloying + heat treatment	Cu–5Cr	850	5.8	/	67	[39]
Rapid solidification + heat treatment Solid solution	Cu-1.3Cr	640	/	210	62	[40]
	Cu-2.5Cr	777	/	260	48	[40]
	Cu-0.8Cr	478	/	185	76	[37]
	Cu-0.8Cr	235	/	/	40	[37]

with the matrix, and it has a completely coherent relationship with the matrix. The precipitation of metastable phases can effectively reduce the elastic strain energy caused by the coherent interface. As the aging process progresses, these metastable phases gradually transform into precipitated phases with stable structures. When the aging temperature is high, the metastable phase is not formed during the supersaturated solid solution decomposition of the alloy, and the body-centered cubic (b.c.c.) Cr phase is directly precipitated.

In the studies of the relationship between the structure and properties of binary alloys, Komen et al. [41–43] believed that the strength of Cu–Cr alloys mainly originated from the dispersed phase. Knight et al. [44] observed the evolution of the precipitated phase of Cu-0.15% Cr alloy during 300–500 °C aging process and found that the alloy precipitated the Cr phase of 5–10 nm even after 500 °C aging for 4 h. Jin et al. [45–48] obtained some conclusions when studying the precipitation process of the Cr phase. Among them, the precipitation sequence of the Cr phase can be summarized as supersaturated solid solution, nano-scale Cr-enriched bundle—Cr-riched G.P. region—coherent b.c.c. structure Cr phase—non-coherent b.c.c. structure Cr phase.

3.1.2. Cu–Cr–Zr

Cu–Cr–Zr alloys actually improve the performance of the alloy by adding a small amount of Zr element and trace amounts of other alloying elements on the basis of Cu–Cr binary system alloys. Among the high-strength and high-conductivity copper alloys, Cu–Cr–Zr alloys have attracted the most attention. Cu–Cr–Zr chemical composition (mass fraction) is 0.25%–1.2% of the content of Cr, 0.08%–0.20% of the content of Zr. The hardness is 78–83 HRB, softening temperature is 550 °C, tensile strength reaches above 600 MPa, and electrical conductivity reaches above 80% IACS. The hardness, strength, electrical conductivity, and thermal conductivity of Cu–Cr–Zr alloys can be significantly improved by the aging treatment. The mechanical and electrical properties of typical Cu–Cr–Zr alloys are shown in Table 2 [49].

The high strength of Cu–Cr–Zr alloy is mainly caused by the dispersed nano-Cr phase. The addition of trace Zr element can not only increase the strength of the alloy, but also affect the precipitation and growth of the Cr phase. As a result, the precipitation process of the alloy becomes more complicated. Tang et al. [56] pointed out that Cr element mainly existed in the G.P. region of black/white petals, and black dot-like contrast in the early aging period. With the progress of the aging, the alloy reaches a peak aging state, at which time the G.P. regions in the alloy are replaced by fine precipitates. The fine precipitates are a Heusler phase with a long-range periodic structure. Its chemical formula is CrCu2(Zr, Mg), and the daughter cell has an N–W relationship with the matrix. When the aging temperature is 500 °C, the precipitated phase begins to grow and gradually loses the coherent relationship with the matrix. When the temperature rises to 550 °C, the precipitates gradually decompose into the coarse Cr phase and Cu_4Zr phase. Batra [57] believed that there were two different forms of Cr phases in Cu-0.8%Cr-0.08%Zr alloys. One was a crude Cr phase which was not dissolved in the solid solution process. The other one was the Cr phase of the b.c.c. structure precipitated during the aging process. According to the diffraction spots of the precipitated phase, the arrangement of the precipitated phase was similar to the Heusler phase, and the chemical formula was CrCu2(Zr). Tenwiek [58] pointed out that Zr mainly existed in the form of Cu_5Zr compound in Cu. The precipitation process of the Cr phase was that Cr element preferentially aggregated and grew on the (001) plane of the matrix and gradually transformed into face-centered cubic (f.c.c.) structure. The Cr phase of the f.c.c. structure was coherent with the matrix. As the aging went on, the precipitates continued to coarsen. In this process, the structure of the Cr phase was transformed from f.c.c. to b.c.c. structure.

Table 2
Mechanical property and electrical conductivity of Cu–Cr–Zr alloys.

Composition /(wt. %)	Strength /MPa)\	Conductivity /(%IACS)	Ref.
Cu-0.4Cr-0.2Zr	637	80	[49]
Cu-0.4 Cr-0.3Zr	568	75.3	[50]
Cu-0.45Cr-0.12Zr	612	78.1	[51]
Cu–1Cr-0.1Zr	690	67	[52]
Cu–1Cr-0.1Zr	648	79.8	[53]
Cu–1Cr-0.1Zr	832	71.2	[54]
Cu–1Cr-0.1Zr	612	84.7	[55]

3.1.3. Cu/Al_2O_3

Cu/Al_2O_3 is one of the most typical dispersion-strengthened copper materials developed since the 1970s. It was first commercialized in the United States and mass-produced under the name “Glidcop”. It is used in applications that require both high electrical conductivity and high-temperature strength. Cu/Al_2O_3 alloy is a new type of composite material with excellent comprehensive physical and mechanical properties. The dispersed phase particles in Cu/Al_2O_3 composite are oxides with a high melting point, high-temperature stability, and high hardness. In 1973, Glidcop Al-10, Glidcop Al-35, and Glidcop Al-60 were launched by the American SCM Company. Their tensile strengths were 500 MPa, 600 MPa, and 620 MPa, respectively, and their electrical conductivities were 92% IACS, 85% IACS, and 80% IACS, respectively.

The dispersion strengthening of Cu/Al_2O_3 composite relies on the *in-situ* reaction to generate a highly heat-resistant and stable nano-reinforced phase Al_2O_3 to greatly strengthen the copper matrix while maintaining the high electrical conductivity. The size of Al_2O_3 must be nano-scale, generally below 50 nm, preferably less than 10 nm. Nano-scale strengthened particles play a strong role in hindering the movement of dislocations and grain boundaries, resulting in Orowan strengthening and fine grain strengthening. Al dispersion-strengthened copper alloys are commonly prepared by

mechanical ball milling hot extrusion method, *in-situ* synthesis, method and internal oxidation method. The properties of Cu/Al_2O_3 composite with different Al_2O_3 contents are shown in Table 3.

Fig. 5 [63] showed the relationship between the tensile strength of Cu/0.5 vol% Al_2O_3 and cold-rolled deformed pure copper as a function of temperature. The tensile strength and yield strength of dispersed copper in the test temperature range were much higher than those of pure copper in comparison. The decrease in the strength of the Cu/Al_2O_3 tended to slow down, and then maintained a linear decrease above 400 °C. This was because the Al_2O_3 particles pin the growth of grains and the movement of dislocations under high-temperature effectively. Guo et al. [64] found that the compressive behavior of this material largely depended on its original microstructure, strain rate, and temperature.

3.1.4. W–Cu

W–Cu material is an incompatible two-phase composite material composed of refractory tungsten and conductive copper. It combines the respective characteristics of tungsten and copper, such as high-temperature strength, high electrical and thermal conductivity, good electrical corrosion resistance, high hardness, low thermal expansion coefficient, and certain plasticity. Moreover, its corresponding mechanical and physical properties can be controlled and adjusted by changing its composition ratio. It has been mainly used as electrical contacts for various high-voltage electrical switches since the 1930s. Because of its high withstand voltage strength and low electrical ablation performance, it has promoted the high-voltage electrical switches to increase the voltage level and power capacity continuously. W–Cu materials were used as electrodes for resistance welding and electrical processing, and used as a protective material exposed to high-temperature gas in aerospace technology. W–Cu materials were used in large-scale integrated circuits as electronic packaging and heat sink materials in the 1990s. The compositions and properties of W–Cu materials for vacuum contacts produced by some factories are shown in Table 4 [65].

Table 3
The properties of Cu/Al_2O_3 composite with different Al_2O_3 contents.

Composition	Strength /MPa	Conductivity /(%IACS)	Ref.
$Cu/2.75Al_2O_3$(vol. %)	570	85	[59]
$Cu/4.5Al_2O_3$(vol. %)	522	90	[60]
$Cu/5Al_2O_3$(vol. %)	650	71.1	[61]
$Cu/0.3Al_2O_3$(vol. %)	440	94.1	[62]

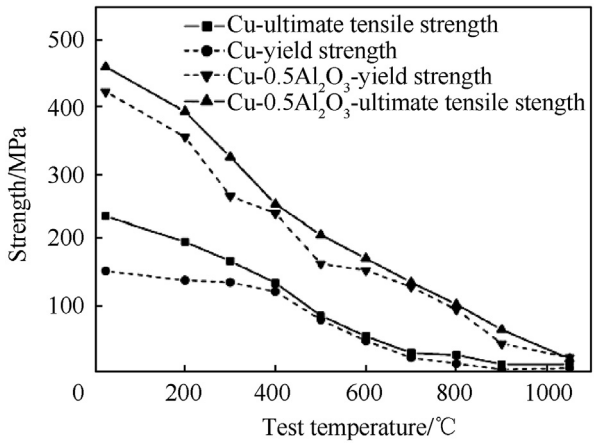

Fig. 5. Yield strength of Cu–0.5 vol% Al_2O_3 composite and several compared materials at elevated temperatures [63].

Due to the large differences in the densification of Cu and W, the dispersion problem has a huge impact on the properties of the composites. Studies have shown that ultrafine nanocomposite powders can significantly reduce the sintering temperature and the activation energy, and promote the sintering process. Zhang et al. [66] used micron-grade industrial copper powder mixed with micron- and nano-sized tungsten powder to prepare Cu–W75 composites. They found that smaller tungsten power led to better performance of the composites. A relative density of 98.9% and a conductivity of 48.7% IACS was obtained when the tungsten powder size reached 400 nm. Cheng et al. [67] used CuO and WO_3 to prepare nano- W–Cu composites by ball milling. The particle sizes of tungsten and copper were less than 100 nm after reduction. W–Cu composites had a relative density of 99% and excellent thermal conductivity and mechanical properties. A novel method of nitridation-denitridation [68] was developed to prepare W–Cu powders including calcination, nitridation, and denitridation. The performance of W–Cu powder mainly depended on the nitridation-denitridation process. The spherical W–Cu powder with a mean particle size of 90.19 nm was obtained when the nitridation temperature and the denitridation temperature were 650 °C and 875 °C, respectively. W–Cu alloys were prepared by sintering the composite powder in hydrogen at 1200 °C for 90 min. The relative density and hardness reached 98.2% and 258.7 HV, respectively.

3.1.5. Mo–Cu

Similar to W–Cu, Mo–Cu is a pseudo-alloy composed of two incompatible metal phases on the structure. It combines the respective performance characteristics and has the advantages of high electrical, thermal conductivity, low thermal expansion coefficient, and good heat resistance. Mo–Cu is used as substrates, inserts, connectors, and heat sinks in large-scale integrated circuits and high-power microwave devices. Mo–Cu material has lower density and easier deformability than W–Cu material. The composition and properties of Mo–Cu materials for vacuum contacts produced by some factories are shown in Table 5 [69].

A. Kumar et al. [70] prepared Mo-20% Cu powder by mechanical alloying. After 40 h of alloying, it was found that the particle size reached about 20 nm, and the distribution became uniform. After X-ray diffraction test, the intensity of the diffraction peak of Cu became smaller, indicating that some Cu was segregated at the grain boundaries of Mo. At this time, the solvent and capacity are in a metastable state, which will greatly improve the sintering activity of the material. It makes the Mo–Cu nano powder reach a higher density at certain sintering temperature. Mo-15 wt.%Cu powder was synthesized by a gelatification-reduction process, in which precursor gelcasts were obtained by adding an initiator into a suspension containing ammonium heptamolybdate, copper oxide, acrylamide organic monomer, and some additives. The gelcasts were then calcined and hydrogen-reduced to convert into Mo–Cu powder. After drying, calcination and reduction, the prepared Mo-15 wt.%Cu powder [71] had a size of 100–200 nm. The powder had extremely high sintering activity. The compacted density of the sintered body reached 98%, flexural strength and electrical conductivity were 833.65 MPa and 41.75%IACS after sintering at 1150 °C for 2 h. Mo–Cu powder with a core-shell structure was fabricated by heterogeneous precipitation and reduction process [72]. After sintered at 1150 °C, the obtained alloy had a density of 97.02%, a hardness of 191.1 HV, and an electrical and thermal conductivity of 27 MS/m and 188.64 $Wm^{-1}K^{-1}$, respectively. The excellent properties were attributed to the core-shell microstructure that almost every Mo particle was capsulated by a continuous network structure of Cu.

Table 4
Compositions and properties of W–Cu materials for vacuum contacts produced by different factories.

Material trademark	Composition /(wt.%)	Hardness /(HV)	Conductivity /(%IACS)	Producer
K10VS	90W–10Cu	313 ± 5	37.9	Austria
K20VS	80W–20Cu	260	43.1	Plansee Co.
K33VS	67W–33Cu	190 ± 20	48.3	
W20CuV	80W–20Cu	220	27.5	German
W35CuV	65W–35Cu	150	39.6	DoDuCo Co.
W35CuSbV	65W–35Cu + Sb	200–240	17.2–27.6	
W10CuV	90W–10Cu	240–260	37.9	Advanced Technology and Materials Co. Ltd.
W15CuV	85W–15Cu	220–240	41.3	

Table 5
Composition and properties of Mo–Cu materials for vacuum contacts produced by some factories.

Material trademark	Composition /(wt.%)	Hardness /(HV)	Conductivity /(%IACS)	Producer
Mo20CuV	80Mo–20Cu	220	27.6	German
Mo25CuV	75Mo–25Cu	180	31	DoDuCo Co.
Mo30CuVS	70Mo–30Cu	170 ± 20	46.5	
Mo35CuV	65Mo–35Cu	150	39.7	
Mo40CuV	60Mo–40Cu	140	44.8	
Mo30CuVS	70Mo–30Cu	170 ± 20	46.5	Austria
Mo40CuVS	60Mo–40Cu	160 ± 20	51.7	Plansee Co.
Mo50CuVS	50Mo–50Cu	150 ± 20	55.2	

3.1.6. Summary of rail materials

At present, many progresses have been made on the composition design, preparation and processing technology of high-strength and high-conductivity copper alloys. The strength and electrical conductivity of copper alloys in various systems are summarized in Fig. 6 for comparison. Those copper alloys have approached their limits of combination properties, based on the literature analysis. It is difficult to further improve the strength and conductivity, unless new materials system or new processing technology is adopted. Although plenty of researches have been done on the hardness, strength and electrical conductivity of various copper alloys, few work is focused on the special environments such as extremely mechanical wear and high temperature thermal shock.

3.2. Application of coating for rails

Copper is most often now used as the choice material for rail applications. The performance of copper, however, has not been fully satisfactory. This is because copper rail surfaces often exhibit severe wear erosion, spark erosion, and pitting processes during the firing of the gun [35]. These wear and erosion effects make the operation of the electromagnetic guns costly and inefficient. These latter deficiencies, such as gouges, grooves, and arc ablation, are even more critical when the electromagnetic railgun is designed to operate in the hypervelocity regime. Electromagnetic guns require the use of materials with a much higher level of thermomechanical stability. Attention is now focused on the application of appropriate coatings on copper to enhance its wear and thermal resistance, and still maintain its excellent electrical and thermal conductivity [35].

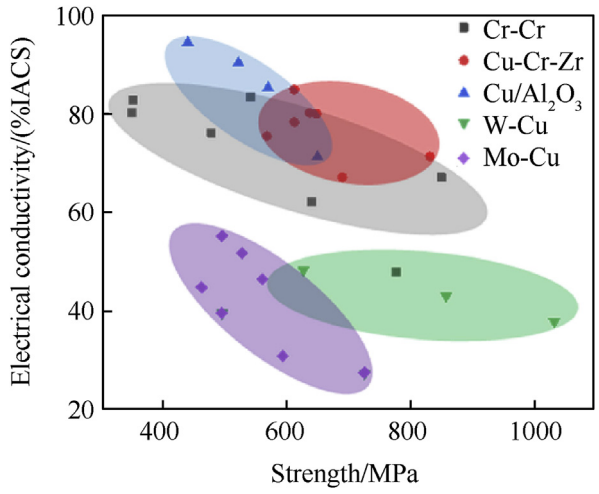

Fig. 6. Comparison of combination properties of electrical conductivity and strength for typical copper alloys (Some strengths are calculated as 3.3 times of the hardness [73]).

James [74] found that the theoretical limit speed of the electromagnetic railgun was related to the skin effect of the speed of the pivot rail material. When the armature reached a certain speed, the armature/rail interface changed from solid/solid contact to liquid/solid contact. The critical speed corresponding to this transition is also called the transition speed, which reflects the basic properties of the armature rail material and determines the armature limit speed. The theoretical calculation results showed that the critical transition speed of pure copper rails was less than 0.5 km/s [74]. If a high melting point Mo or W was wrapped on the surface of pure copper rails, the critical transition speed could be increased to more than 2 km/s. This study provided a new idea for increasing the limit speed of the armature, that is, the surface of pure copper rails was wrapped with a high melting point Mo or W material, and the thickness of the rails coating layer was optimized to meet the requirements of the thermal environment without seriously damaging the electromagnetic field.

Siopis et al. [22] considered the material of the guide rail and adopted a systematic material selection (Ashby method). They believed that the guide rail mainly had three failure modes such as gouges, grooves, and fractures. Resistivity is the key factor affecting electromagnetic energy while tensile strength, melting point, and elongation are the main factors affecting the failure. Fig. 7 showed a multi-objective trade-off diagram and a schematic diagram of potential mixed materials [22]. The lower the value in the trade-off diagram, the more feasible it is. After analysing and comparing the existing 2790 kinds of materials, it was found that no single material could match well. After considering different material composite models, it is concluded that the overlay structure can achieve the best match of two key factors. The cladding structure proposed by Siopis refers to a composite structure with copper alloy as the conductive substrate and tungsten, chromium, nickel,

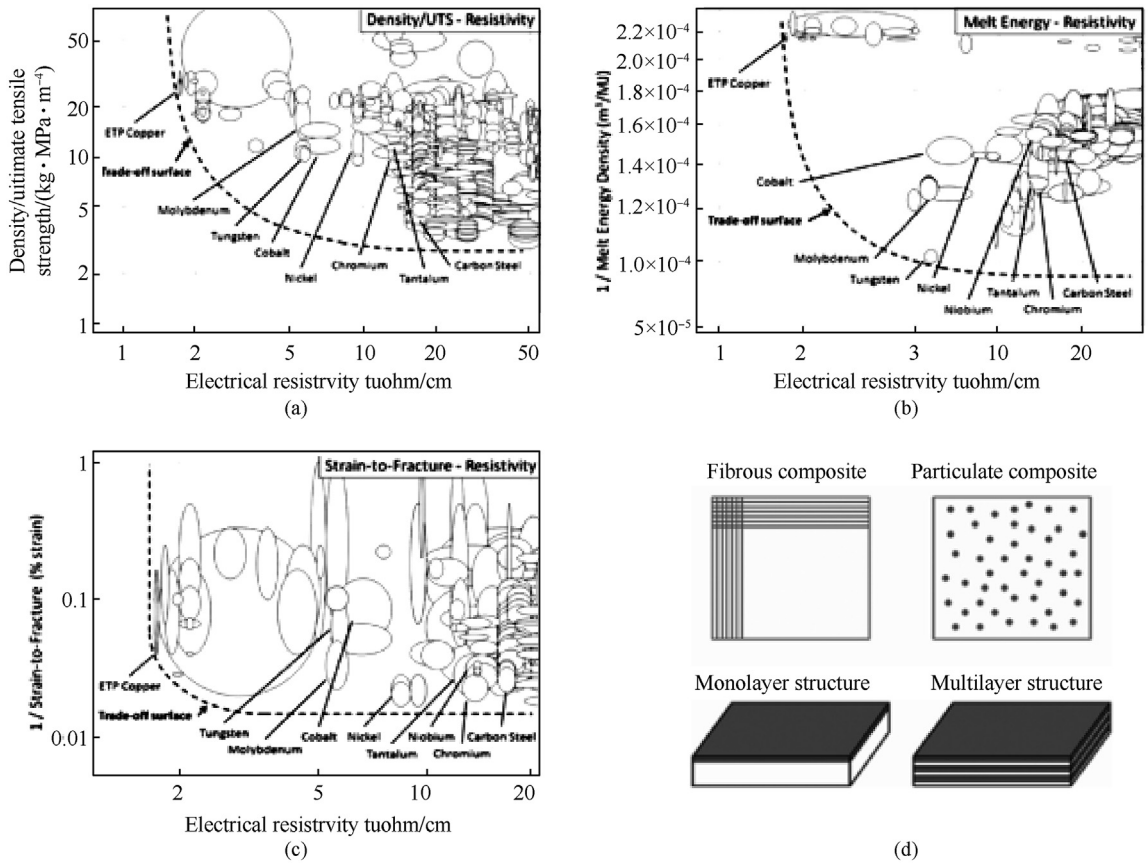

Fig. 7. Multi-objective trade-off diagram and schematic diagram of potential hybrid materials. (a) Magnetic energy (electrical resistivity) and rail durability (density/UTS); (b) magnetic energy (electrical resistivity) and durability (melt energy density); (c) magnetic energy (electrical resistivity) and rail durability (strain-to-fracture); (d) Four potential hybrid material configurations [22].

or tantalum as the damage-resistant surface layer.

Based on the above theoretical analysis results, various researchers have proposed a variety of cladding structure guide rails, using different surface strengthening technologies to improve the wear resistance and ablation resistance of the track surface.

3.2.1. Electroplating

Electroplating is a surface treatment method that deposits and forms a coating on the surface of a substrate by the principle of electrolysis. Silver-cyanide-free plating was performed in a thiosulfate bath containing the main salts of $AgNO_3$ and AgBr, respectively [75]. The obtained Ag coating had nano crystal grains with an average size of 55 nm. Compared with the bath containing AgBr main salt, the bath containing $AgNO_3$ main salt has a larger current density range, and the corresponding Ag coating has higher microhardness and smaller grain size. Lv et al. [76] studied the graphite-reinforced Ag-based composite coating by a composite electrodeposition method, and the friction coefficient was reduced by 70% compared with the silver coating.

McNeal [77] compared the damage of Cu–W rails, chrome-plated Cu–W rails, and chrome-plated pure Cu rails after multiple launches. It was found that chrome-plated pure Cu rails suffered the most damage, while chrome-plated Cu–W rails suffered the least damage. Castro-Dettmer et al. [78] observed that cracks and holes appeared in the chromium layer. The heat emission effect reduces the hardness of the coating and the substrate. The cracking of the chromium coating was produced by the mismatch of the thermal expansion coefficients of chromium and copper. Additionally, the erosion of the Cu substrate by the molten Al through the cracks of the chromium coating is an important factor that reduces the life of the rail as shown in Fig. 8.

3.2.2. Cold spraying

Cold spraying is a thermal spraying technique based entirely on aerodynamic principles. During the spraying process, the particles collide with the substrate at very high speed (300–1200 m/s), and the coating is deposited by forming a strong plastic deformation. When using this technology to prepare conductive wear-resistant self-lubricating coatings, particles do not undergo melting-resolidification during flight and deposition due to the low working temperature (100–600 °C). Therefore, particle oxidation and phase defects are avoided and the conductive properties of the coating are maintained.

Tazegul et al. [79] used a cold spraying process to add Al_2Cu particles in copper-based coatings. The bonding effect between Al_2Cu particles and Cu particles was enhanced, and chemical compatibility was good. The friction coefficient of the coating containing 10% Al_2Cu decreased by 33%, and the wear rate decreased by 80%. Tazegul et al. [80] also used cold spraying to prepare a SiC-reinforced copper-based composite coating on the surface of pure copper. As the SiC content of the hard particles increased, the wear resistance of the coating improved.

3.2.3. Supersonic plasma spraying

Supersonic plasma spraying uses a rigid non-transferable plasma arc as a heat source to heat the working gas to form a high-temperature and high-speed plasma jet, thereby heating, accelerating, and forming a molten particle stream of the powder in the incident stream. Since the temperature of the plasma jet can reach tens of thousands of degrees Celsius, coatings such as

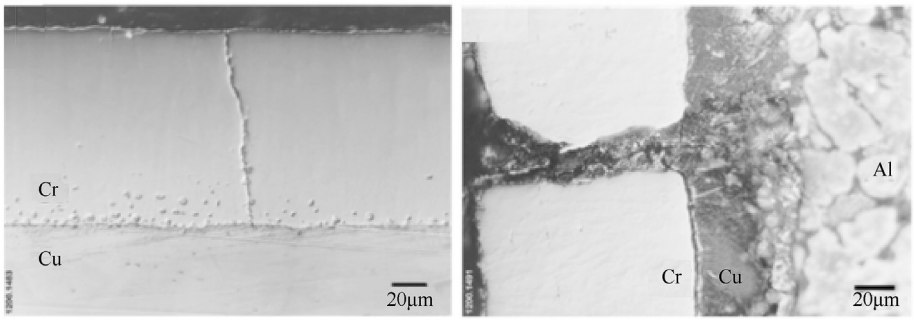

Fig. 8. Cracks on the surface of the chrome plating of pure Cu rails and the microstructure of liquid Al eroded the Cu matrix through cracks [78].

refractory metals and oxide ceramics and cermets can be prepared using plasma spray technology.

Liu et al. [81,82] used a supersonic plasma spraying technique to prepare a Mo-based coating on the surface of a copper rail. The conductivity of the coating was 6.01% IACS, and the micro-hardness was 482.3$HV_{0.1}$. The addition of the W element improved the micro-hardness of the coating, suppressed the occurrence of planning and scratches, and also enhanced its wear resistance. After current-carrying friction and wear tests, the surface of the Mo–W coating experienced adhesive wear, abrasive wear, and arc ablation wear.

3.2.4. Laser cladding

Laser cladding is a method of adding a cladding material and using a high-energy-density laser beam to fuse it to form a metallurgical additive cladding layer on the surface of the substrate. As an important means of surface modification, laser cladding has the advantages of high flexibility, small thermal influence on the workpiece, and high bonding strength between the coating and the substrate. Therefore, it is widely used in metal surface modification of materials. A fine-grained, high-performance coating can be obtained by this technique. However, it is difficult to perform laser cladding on the copper surface because copper has a high reflectivity to laser light. Many scholars have carried out a series of researches on this problem.

Bysakh et al. [83] used an 8 kW CO_2 laser to prepare alloyed layers of Cu–Fe–Al–Si. The formation of micron-level iron-rich balls with DO_3 structure in the copper-rich f.c.c. matrix indicated that the immersed miscible gap was approached during laser processing. In the later stages of solidification, the solute rejection process resulted in the evolution of submicron-sized copper-rich dispersions within the iron-rich spheres. Zhang et al. [84] successfully deposited nickel-based alloy coating onto a pure copper surface by laser cladding with coaxial powder feeding. X-ray diffraction analysis results showed that the coating was mainly composed of γ- (Ni, Cr, Mo, W) solid solution, some carbides, and silicides. The average hardness of the coating was about 360 $HV_{0.1}$, which was about five times that of pure copper. The dry sliding wear test showed that the wear resistance of the copper was significantly improved after laser cladding. Dehm et al. [85] prepared a Cu–Ni–B–Si intermediate layer by plasma spraying on a pure copper substrate, and then prepared a Co-based hardfacing on the intermediate layer. The matrix of the coating was β-Co as it was alloyed with Mo, Cr and Si and combined with rapid cooling. Yan et al. [86] successfully prepared a Ni–Cr/TiB_2 metal matrix composite (MMC) coating with a small amount of CaF_2 on a Cu–Cr–Zr alloy substrate by laser cladding. The microstructure of the coating was mainly composed of dendrites, cystiform-dendrites, and particles. By increasing the content of TiB_2 to 20 wt%, the dendritic microstructural features transformed into particles. Compared with a pure copper substrate, laser cladding Ni–Cr/TiB_2 MMC coating on copper had higher micro-hardness and better wear resistance. The highest micro-hardness was 946 $HV_{0.1}$, which was eight times higher than the original substrate. The coefficient of friction of the coating was significantly reduced to about 0.24, and a relatively smooth wear surface was observed. Ng et al. [87] used laser cladding technology to form a Mo/Ni/Cu "sandwich" structure coating on a Cu substrate. The introduction of Ni in the intermediate layer greatly alleviated the problems of large differences in thermal properties and low mutual solubility between Cu and Mo. As the hardness of the modified layer increased, the wear resistance was also increased by 7 times. The average resistance of the modified layer was measured to be $2.5 \times 10^{-7}\ \Omega \cdot cm^{-2}$. Li et al. [88] used laser surface modification technology to form a nickel-based (NiCrBSi) modified layer doped with Ta_2O_5 + C powder. Fig. 9 shows the magnified scanning electron microscope (SEM) micrograph and

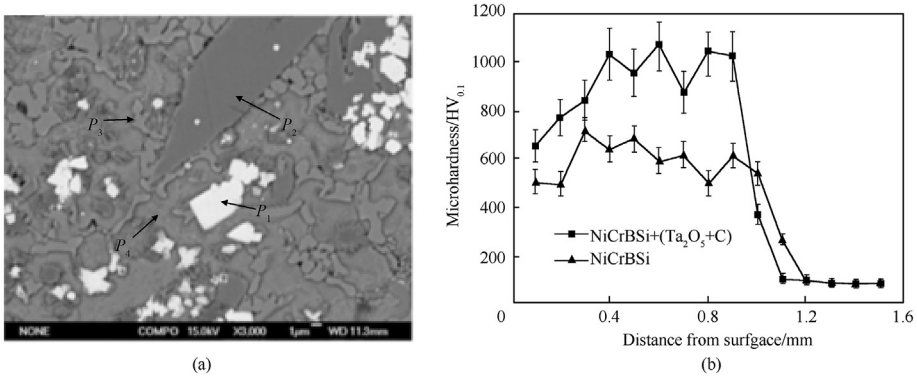

Fig. 9. Modified layer (a) magnified SEM micrograph; (b) micro-hardness profile along the cross-section [88].

Table 6
The overall design requirements and solutions of the rail materials.

Railgun requirements	Maximized magnetic energy		Maximized durability	
Service environment	Large electrical currents			
	Large electro-magnetic loads	High local temperatures	High sliding velocities	
Challenges	Bending	Grooves	Gouges	Transition and arc ablation
Rail requirements	High strength	High thermal conductivity	High hardness	High resistance to arc ablation
Status	Partly solved		Little solved	
Solutions	Development of high-strength and high-conductivity rails		Application of coatings on rails	
Trends	Approach the limit		A fresh area	

micro-hardness profile along cross-section of the modified layer. A granular TaC phase (P1) and a coarse needle-like Cr_3C_2 phase (P2) were formed. The TaC particles synthesized *in situ* were uniformly dispersed in γ (Ni, Fe) solid solution (P3) and (Cu, Ni, Fe) solid solution (P4). It was found that the bonding strength between the modified layer and the matrix increased, and the surface hardness increased to 918 $HV_{0.1}$. The conductivity was 84.5% IACS and the wear resistance was 2.5 times higher than the sample without coating.

3.2.5. Summary of surface coating

The four kinds of surface modification techniques on copper alloys are introduced. Among them, laser cladding technology is a promising surface treatment technology due to its high flexibility, small thermal influence and large adjustable range of coating thickness. At present, the research on the preparation process and microscopic mechanism of copper alloy coatings is still in its infancy. In particular, mechanical and thermal shock tests of surface coatings to simulate electromagnetic emission processes are still lacking.

4. Conclusions and prospects of rail materials

In this study, different failure mechanisms of rail materials are analyzed. In consideration of magnetic efficiency and durability, the rail material should have the following requirements: high electrical conductivity, high hardness, high thermal conductivity and high resistance to abrasion and arc ablation. The conducting rails of most of electromagnetic launchers have been copper alloys (Cu–Cr, Cu–Cr–Zr, Cu–W and Cu/Al_2O_3) for their excellent electrical and thermal conductivity with great magnetic efficiency. The performance of copper alloys, however, has not been fully satisfactory with durability (also known as service life). Attention is now focused on the application of appropriate coatings on copper using different surface strengthening technologies (electroplating, cold spray, supersonic plasma spraying and laser cladding) to improve both efficiency and durability. The overall design requirements and solutions of the rail materials are summarized in Table 6.

Considering that the development of high-strength and high-conductivity alloys has almost approached the limit, the main research and development prospects of rail materials are suggested as follows.

(1) The composite structure can indeed improve the properties of the copper alloy to a certain extent, but it is also necessary to consider the properties matching between the cladding material and the copper matrix. Otherwise, failures such as cracks of the coating are prone to occur in service on the actual track.
(2) From the perspective of the materials currently studied, Ni, Mo, and W coatings and ceramics are the preferred series of coating materials. However, new materials with integrated conductive wear resistance and ablation resistance should be explored to further optimize the quality of the coating.
(3) The understanding of the conductive wear resistance and ablation resistance of the coating should be deepened. The mechanism of current-carrying tribology of the coating under severe working conditions and the mechanism of the arc ablation under extreme conditions are highly required.
(4) Standard methods for friction and wear tests under high-speed, current-carrying, and magnetic-field conditions should be developed.

Declaration of competing interest

The authors declare that they have no known competing financial interests or personal relationships that could have appeared to influence the work reported in this paper.

Acknowledgment

This work is supported by the National Key R&D Program of China (No. 2017YFB1200800), the National Natural Science Foundation of China (No. 11725210, 11572281, 51827810, 51637009), the Fundamental Research Funds for the Central Universities (2018XZZX001-05) and the National Student's Platform for Innovation and Entrepreneurship Training Program (201910335115).

References

[1] Ma W, Lu J. Thinking and study of electromagnetic launch technology. IEEE Trans Plasma Sci 2017;45:1071–7.
[2] Watt T, Motes DT. The effects of surface coatings on the onset of rail gouging. IEEE Trans Plasma Sci 2010;39:168–73.
[3] Graff KF, Dettloff BB. The gouging phenomenon between metal surfaces at very high sliding speeds. Wear 1969;14:87–97.
[4] Barber JP, Bauer DP. Contact phenomena at hypervelocities. Wear 1982;78:163–9.
[5] Stefani F, Parker JV. Experiments to measure gouging threshold velocity for various metals against copper. IEEE Trans Magn 1999;35:312–6.
[6] Tarcza K, Weldon W. Metal gouging at low relative sliding velocities. Wear 1997;209:21–30.
[7] Schneider M, Schneider R. Advanced rail-sabot configurations for brush armatures. IEEE Trans Magn 2006;43:186–9.
[8] Cooper KP, Jones HN, Meger RA. Analysis of railgun barrel material. IEEE Trans Magn 2007;43:120–5.
[9] Gee RM, Persad C. The response of different copper alloys as rail contacts at the breech of an electromagnetic launcher. IEEE Trans Magn 2001;37:263–8.
[10] Meger R, Cooper K, Jones H, Neri J, Qadri S, Singer I, et al. Analysis of rail surfaces from a multishot railgun. IEEE Trans Magn 2005;41:211–3.
[11] Stefani F, Merrill R. Experiments to measure melt-wave erosion in railgun armatures. IEEE Trans Magn 2003;39:188–92.
[12] Cooper KP, Jones HN, Meger RA. Analysis of railgun barrel material. IEEE Trans Magn 2006;43:120–5.
[13] Watt T, Stefani F, Crawford M, Mark H, Parker J. Investigation of damage to solid-armature railguns at startup. IEEE Trans Magn 2006;43:214–8.
[14] Persad C. Solid armature performance: a progress review 1980-1990. IEEE Trans Magn 1997;33:134–9.
[15] Tang B, Xu Y, Lin Q, Li B. Synergy of melt-wave and electromagnetic force on the transition mechanism in electromagnetic launch. IEEE Trans Plasma Sci 2017;45:1361–7.
[16] Parks PB. Current melt-wave model for transitioning solid armature. J Appl Phys 1990;67:3511–6.
[17] Benton T, Stefani F, Satapathy S, Hsieh K-T. Numerical modeling of melt-wave erosion in conductors [railgun armatures]. IEEE Trans Magn 2003;39:129–33.
[18] Woods LC. The current melt-wave model. IEEE Trans Magn 1997;33:152–6.

[19] Stefani F, Levinson S, Satapathy S, Parker J. Electrodynamic transition in solid armature railguns. IEEE Trans Magn 2001;37:101–5.
[20] Barber JP, McNab IR. Magnetic blow-off in armature transition. IEEE Trans Magn 2003;39:42–6.
[21] Satapathy S, Vanicek H. Down-slope contact transition in railguns. IEEE Trans Magn 2006;43:402–7.
[22] Siopis MJ, Neu RW. Materials selection exercise for electromagnetic launcher rails. IEEE Trans Magn 2013;49:4831–8.
[23] Persad C, Marshall R, Alien R, Barton A, Wright D, Eliezer Z. A comparison of the wear behaviors of six elemental wire conductors. IEEE Trans Magn 1995;31:746–51.
[24] Day M, Baker MC, Grant G. HERA railgun facility at Texas Tech University. IEEE Trans Magn 1993;29:787–91.
[25] Persad C, Lund C, Eliezer Z, Peterson D, Hahne J, Zowarka R. Wear of conductors in railguns: metallurgical aspects. IEEE Trans Magn 1989;25:433–7.
[26] An X, Wu S, Wang Z, Zhang Z. Significance of stacking fault energy in bulk nanostructured materials: insights from Cu and its binary alloys as model systems. Prog Mater Sci 2019;101:1–45.
[27] An XH, Wu SD, Zhang ZF, Figueiredo RB, Gao N, Langdon TG. Enhanced strength–ductility synergy in nanostructured Cu and Cu–Al alloys processed by high-pressure torsion and subsequent annealing. Scripta Mater 2012;66:227–30.
[28] Matyac MJ, Christopher F, Jamison KA, Persad C, Marshall RA. Railgun performance enhancement from distribution of energy feeds. IEEE Trans Magn 1995;31:332–7.
[29] Hurn T, D'Aoust J, Sevier L, Johnson R, Wesley J. Development of an advanced electromagnetic gun barrel. IEEE Trans Magn 1993;29:837–42.
[30] Hammon H, Dempsey J, Strachan D, Raos R, Haugh D, Whitby F, et al. The Kirkcudbright electromagnetic launch facility. IEEE Trans Magn 1993;29:975–9.
[31] Wolfe T, Spiegelberg W, Evangelist M. Exploratory metallurgical evaluation of worn rails from a 90 mm electromagnetic railgun. IEEE Trans Magn 1995;31:770–5.
[32] Bedford A. Rail damage and armature parameters for different railgun rail materials. IEEE Trans Magn 1984;20:352–5.
[33] Schulman MB, Wootton RE, Stefani F, Fikse DA, Docherty EF, DeMarchi VF. HART hypervelocity augmented railgun test facility. IEEE Trans Magn 1993;29:505–10.
[34] Hahne JJ, Herbst J, Upshaw J. Fabrication and testing of a 30 mm and 90 mm laminated, high L'railgun designed and built at CEM-UT. IEEE Trans Magn 1995;31:303–8.
[35] Colombo GR, Otooni M, Evangelisti MP, Colon N, Chu E. Application of coatings for electromagnetic gun technology. IEEE Trans Magn 1995;31:704–8.
[36] Liao S, Yin Z, Jiang Q, Jiang F, Song L, Wang M. Effect of heat treatment on mechanical properties and electrical conductivity of Cu-Cr(-Zr)alloy. Chin J Nonferrous Met. 2000:684–7.
[37] Ping L, Kang B, Cao X, Huang J, Gu H. Coherent strengthening of aging precipitation in rapidly solidified Cu-Cr alloy. Acta Metall 1999:561–4.
[38] Xu S, Fu H, Wang Y, Xie J. Effect of Ag addition on the microstructure and mechanical properties of Cu-Cr alloy. Mater Sci Eng A 2018;726:208–14.
[39] Zhang, Guofeng, Li Z, Wang, Erde, Liang, Guoxian. Structure and properties of the mechanically alloyed Cu-5Cr Alloy. P/M Technol. 1996:175–80.
[40] Uchida S, Kimura T, Nakamoto T, Ozaki T, Miki T, Takemura M, et al. Microstructures and electrical and mechanical properties of Cu-Cr alloys fabricated by selective laser melting. Mater Des 2019;175:107815.
[41] Komem Y, Rezek J. Precipitation at coherency loss in Cu-0.35 wt pct Cr. Metall Trans A 1975;6:549.
[42] Zhang D, Mihara K, Takakura E, Suzuki H. Effect of the amount of cold working and ageing on the ductility of a Cu–15% Cr–0.2% Ti in-situ composite. Mater Sci Eng A 1999;266:99–108.
[43] Fujii T, Nakazawa H, Kato M, Dahmen U. Crystallography and morphology of nanosized Cr particles in a Cu–0.2% Cr alloy. Acta Mater 2000;48:1033–45.
[44] Knights R, Wilkes P. Precipitation of chromium in copper and copper-nickel base alloys. Metall Trans 1973;4:2389–93.
[45] Jin Y, Adachi K, Suzuki H, Takeuchi T. Correlation between the cold-working and aging treatments in a Cu-15 Wt Pct Cr in situ composite. Metall Mater Trans 1998;29:2195–203.
[46] Jin Y, Adachi K, Takeuchi T, Suzuki H. Cu precipitation in Cr ribbon of Cu-15 wt % Cr in situ composite. Appl Phys Lett 1996;69:1391–2.
[47] Jin Y, Adachi K, Takeuchi T, Suzuki H. Correlation between the electrical conductivity and aging treatment for a Cu-15 wt% Cr alloy composite formed in-situ. Mater Lett 1997;32:307–11.
[48] Jin Y, Adachi K, Takeuchi T, Suzuki H. Ageing characteristics of Cu–Cr in-situ composite. J Mater Sci 1998;33:1333–41.
[49] Jiang F, Chen X, Chen M, Jiang L, Xiang Z, Wang W. Research progress in nanosized precipitation and phase mechanism of high-strength and high-conductivity Cu-Cr-Zr alloy. Mater Rep 2009;23:72–6.
[50] Meng A, Nie J, Wei K, Kang H, Liu Z, Zhao Y. Optimization of strength, ductility and electrical conductivity of a Cu–Cr–Zr alloy by cold rolling and aging treatment. Vacuum 2019;167:329–35.
[51] Liang N, Liu J, Lin S, Wang Y, Wang JT, Zhao Y, et al. A multiscale architectured CuCrZr alloy with high strength, electrical conductivity and thermal stability. J Alloys Compd 2018;735:1389–94.
[52] Zhang S, Li R, Kang H, Chen Z, Wang W, Zou C, et al. A high strength and high electrical conductivity Cu-Cr-Zr alloy fabricated by cryorolling and intermediate aging treatment. Mater Sci Eng A 2017;680:108–14.
[53] Li R, Guo E, Chen Z, Kang H, Wang W, Zou C, et al. Optimization of the balance between high strength and high electrical conductivity in CuCrZr alloys through two-step cryorolling and aging. J Alloys Compd 2019;771:1044–51.
[54] Zhang ZY, Sun LX, Tao NR. Nanostructures and nanoprecipitates induce high strength and high electrical conductivity in a CuCrZr alloy. J Mater Sci Technol 2020;48:18–22.
[55] Huang AH, Wang YF, Wang MS, Song LY, Li YS, Gao L, et al. Optimizing the strength, ductility and electrical conductivity of a Cu-Cr-Zr alloy by rotary swaging and aging treatment. Mater Sci Eng A 2019;746:211–6.
[56] Tang N, Taplin D, Dunlop G. Precipitation and aging in high-conductivity Cu–Cr alloys with additions of zirconium and magnesium. Mater Sci Technol 1985;1:270–5.
[57] Batra I, Dey G, Kulkarni U, Banerjee S. Microstructure and properties of a Cu–Cr–Zr alloy. J Nucl Mater 2001;299:91–100.
[58] Tenwick M, Davies H. Enhanced strength in high conductivity copper alloys. Mater Sci Eng 1988;98:543–6.
[59] Zhang X-H, Li X-X, Chen H, Li T-B, Su W, Guo S-D. Investigation on microstructure and properties of Cu–Al2O3 composites fabricated by a novel in-situ reactive synthesis. Mater Des 2016;92:58–63.
[60] Li C, Xie Y, Zhou D, Zeng W, Wang J, Liang J, et al. A novel way for fabricating ultrafine grained Cu-4.5 vol% Al2O3 composite with high strength and electrical conductivity. Mater Char 2019;155:109775.
[61] Zhou D, Wang X, Muránsky O, Wang X, Xie Y, Yang C, et al. Heterogeneous microstructure of an Al2O3 dispersion strengthened Cu by spark plasma sintering and extrusion and its effect on tensile properties and electrical conductivity. Mater Sci Eng A 2018;730:328–35.
[62] Ren F, Zhi A, Zhang D, Tian B, Volinsky AA, Shen X. Preparation of Cu–Al2O3 bulk nano-composites by combining Cu–Al alloy sheets internal oxidation with hot extrusion. J Alloys Compd 2015;633:323–8.
[63] Tian B, Liu P, Song K, Li Y, Liu Y, Ren F, et al. Microstructure and properties at elevated temperature of a nano-Al2O3 particles dispersion-strengthened copper base composite. Mater Sci Eng A 2006;435:705–10.
[64] Guo MX, Wang MP. The compression characteristics of particle-containing Cu alloys under different conditions. Mater Sci Eng A 2012;556:807–15.
[65] Zhou W, Lu D. Development of application and production in W-Cu materials. Mater Sci Eng Powder Met 2005:21–5.
[66] Zhang Q, Liang S, Hou B, Zhuo L. The effect of submicron-sized initial tungsten powders on microstructure and properties of infiltrated W-25 wt.% Cu alloys. Int J Refract Metals Hard Mater 2016;59:87–92.
[67] Cheng J, Song P, gong Y, Cai Y, Xia Y. Fabrication and characterization of W–15Cu composite powders by a novel mechano-chemical process. Mater Sci Eng A 2008;488:453–7.
[68] Wei X, Tang J, Ye N, Zhuo H. A novel preparation method for W–Cu composite powders. J Alloys Compd 2016;661:471–5.
[69] Han S, Song Y, Cui S, Xia Y, Zhou Z, Li M. Research and development of Mo-Cu alloy. Powder Metall Ind 2007:40–5.
[70] Kumar A, Jayasankar K, Debata M, Mandal A. Mechanical alloying and properties of immiscible Cu-20 wt.% Mo alloy. J Alloys Compd 2015;647:1040–7.
[71] Song P, Cheng J, Wan L, Zhao J, Wang Y, Cai Y. Preparation and characterization of Mo-15 Cu superfine powders by a gelatification-reduction process. J Alloys Compd 2009;476:226–30.
[72] Wang D, Yin B, Sun A, Li X, Qi C, Duan B. Fabrication of Mo–Cu composite powders by heterogeneous precipitation and the sintering properties of the composite compacts. J Alloys Compd 2016;674:347–52.
[73] Yao GC, Mei QS, Li JY, Li CL, Ma Y, Chen F, et al. Cu/C composites with a good combination of hardness and electrical conductivity fabricated from Cu and graphite by accumulative roll-bonding. Mater Des 2016;110:124–9.
[74] James T. Performance criteria for EM rail launchers with solid or transition armatures and laminated rails. IEEE Trans Magn 1991;27:482–7.
[75] Ren F-z, Yin L-t, Wang S-s, Volinsky AA, Tian B-h. Cyanide-free silver electroplating process in thiosulfate bath and microstructure analysis of Ag coatings. Trans Nonferrous Met Soc China 2013;23:3822–8.
[76] Lv W, Chen TS, Zheng KQ, Zhang ZG. Feasible preparation and improved properties of Ag-graphite composite coating for switch contact by cyanide-free electrodeposition. Mater Corros 2018;69:933–40.
[77] McNeal CJ. Barrel wear reduction in rail guns: the effects of known and controlled rail spacing on low voltage electrical contact and the hard chrome plating of copper-tungsten rail and pure copper rails: monterey, California. Naval Postgraduate School; 2003.
[78] Castro-Dettmer Z, Gee RM, Persad C. Post-test characterization of a chromium-plated copper conductor. Mater Char 1999;43:251–8.
[79] Tazegul O, Dylmishi V, Cimenoglu H. Copper matrix composite coatings produced by cold spraying process for electrical applications. Arch Civ Mech Eng 2016;16:344–50.
[80] Tazegul O, Meydanoglu O, Kayali ES. Surface modification of electrical contacts by cold gas dynamic spraying process. Surf Coating Technol 2013;236:159–65.
[81] Liu G, Yang X, Zhang Y, Yan T, Wei M. Research on microstructure and properties of supersonic plasma sprayed Mo coating based on orthogonal experiment. Acta Armamentarii 2016;37:1489–96.
[82] Yan T, Liu G, Wu H, Zhu S, Liu M. Mechanical properties of Mo-W coatings prepared by supersonic plasma spraying. China Surf Eng 2017;30:107–14.
[83] Bysakh S, Chattopadhyay K, Maiwald T, Galun R, Mordike BL. Microstructure evolution in laser alloyed layer of Cu–Fe–Al–Si on Cu substrate. Mater Sci Eng

A 2004;375–377:661–5.
[84] Zhang Y-z, Tu Y, Xi M-z, Shi L-k. Characterization on laser clad nickel based alloy coating on pure copper. Surf Coating Technol 2008;202:5924–8.
[85] Dehm G, Bamberger M. Laser cladding of Co-based hardfacing on Cu substrate. J Mater Sci 2002;37:5345–53.
[86] Yan H, Zhang P, Yu Z, Lu Q, Yang S, Li C. Microstructure and tribological properties of laser-clad Ni–Cr/TiB2 composite coatings on copper with the addition of CaF2. Surf Coating Technol 2012;206:4046–53.
[87] Ng KW, Man HC, Cheng FT, Yue TM. Laser cladding of copper with molybdenum for wear resistance enhancement in electrical contacts. Appl Surf Sci 2007;253:6236–41.
[88] Li MY, Chao MJ, Liang EJ, Li DC, Yu JM, Zhang JJ. Laser synthesised TaC for improving copper tribological property. Surf Eng 2013;29:616–9.